Size-consistent implementation of Hamiltonian simulation-based quantum-selected configuration interaction method for the supramolecular approach

Kenji Sugisaki^{1,2,*}

¹Deloitte Tohmatsu Financial Advisory LLC, 3-2-3 Marunouchi, Chiyoda-ku, Tokyo 100-8363, Japan

²Centre for Quantum Engineering, Research and Education (CQuERE),

TCG Centres for Research and Education in Science and Technology

(TCG CREST), Sector V, Salt Lake, Kolkata 700091, India

(Dated: October 28, 2025)

The quantum-selected configuration interaction (QSCI) method is a promising approach for large-scale quantum chemical calculations on currently available quantum hardware. However, its naive implementation lacks size consistency, which is essential for accurate intermolecular interaction energy calculations using the supramolecular approach. Here, we present a size-consistent implementation of QSCI by sampling Slater determinants for the dimer in the localized molecular orbital basis, constructing the subspaces for the monomers and dimer, and augmenting the dimer subspace with additional determinants required for size consistency. Implemented within the Hamiltonian simulation-based QSCI (HSB-QSCI) framework, our method numerically satisfies size consistency for 4H/8H clusters, the FH dimer, and the FH-H₂O system. Application to intermolecular interaction energy calculations of hydrogen-bonded FH dimer and FH-H₂O demonstrates that our approach reproduces complete active space-configuration interaction (CAS-CI) values with errors below $0.04~\rm kcal~mol^{-1}$.

I. INTRODUCTION

Quantum computation holds the potential to revolutionize our society. Among its diverse applications, sophisticated quantum chemical calculations are considered one of the most promising. Accurate quantum chemical calculations can accelerate drug and materials discovery, elucidate reaction mechanisms in enzymes and biomolecules, and so on. Quantum phase estimation (QPE) [1–3] and variational quantum eigensolver (VQE) [4] are two major quantum computational approaches, targeting the fault-tolerant quantum computing (FTQC) and noisy intermediate-scale quantum (NISQ) eras, respectively, and both methods have been extensively investigated from theoretical and hardware demonstration perspectives. However, QPE typically requires quantum circuit that are prohibitively deep for even the most advanced quantum hardware available today, rendering its application to industrially relevant molecules extremely challenging until FTQC becomes a reality. On the other hand, VQE can be executed on NISQ devices, but it faces several significant challenges, such as substantial measurement overhead [5], the presence of barren plateaus [6], and so on.

The quantum-selected configuration interaction (QSCI) method was proposed to perform large-scale quantum chemical calculations using currently available quantum hardware [7]. In QSCI, a quantum computer is used to sample Slater determinants that make significant contributions to the wave function of the target electronic state. The information from these sampled Slater determinants is then transferred to a classical computer,

where the subspace Hamiltonian is constructed and diagonalized to obtain the energy and wave function. The key step in QSCI is the preparation of a quantum state suitable for sampling important Slater determinants. Initially, quantum state preparation methods based on VQE and adiabatic state preparation were proposed for this purpose [7]. In 2025, Robledo-Moreno and coworkers introduced a method for quantum state preparation based on the local unitary cluster Jastrow (LUCJ) ansatz [8] with classically computed coupled cluster singles and doubles (CCSD) excitation amplitudes. They demonstrated QSCI calculations using up to 77 qubits on superconducting quantum processors, aided by an error mitigation technique called self-consistent configuration recovery [9]. Recently, we proposed a quantum state preparation method for OSCI based on Hamiltonian simulation (HSB-QSCI) [10], in which important Slater determinants are sampled from quantum states generated by real-time evolution of an approximate wave function. HSB-QSCI offers several advantages over the original QSCI: (1) a simple wave function such as a Hartree-Fock (HF) wave function can be used as the initial state for time evolution, (2) VQE variational optimization is not required, (3) different samples can be obtained by varying the evolution time, (4) long-time evolution is challenging to simulate on classical computers, and (5) higher-order excited configurations can be sampled even with shorter evolution times. We have also reported proof-of-principle demonstrations of HSB-QSCI for one-dimensional carbon chain molecules (carbynes), utilizing up to 36 qubits of an IBM superconducting quantum processor, with the aid of matrix product operator (MPO)-based classical optimization of the quantum circuit for the time evolution operator [11]. Shortly after our publication, methods based on the same concept were reported by

^{*} kensugisaki@tohmatsu.co.jp

other groups [12–14]. Notably, Weaving and coworkers reported that time evolution-based state preparation for QSCI yields a more compact wave function expansion than conventional selected CI in SiH_4 system [15].

Although QSCI has been actively investigated from both theoretical and experimental perspectives [16–32], it suffers from a serious drawback: QSCI is not size consistent unless special care is taken. In its naive implementation, the energy of a dimer composed of non-interacting monomers is generally not equal to the sum of the energies of the individual monomers. In fact, as discussed in the Supporting Information, the number of quantum circuit executions must increase exponentially with system size even approximately satisfy the size consistency condition. Consequently, the straightforward application of QSCI to the calculation of intermolecular interaction energies using the supramolecular approach is fundamentally impractical. In the supramolecular approach, the intermolecular interaction energy $E_{\rm int}$ is calculated using the following equation:

$$E_{\rm int} = E_{\rm AB} - E_{\rm A} - E_{\rm B} \tag{1}$$

Here, $E_{\rm A}$, $E_{\rm B}$, and $E_{\rm AB}$ represent the energies of monomer A, monomer B, and the interacting dimer (A + B), respectively. To address the challenges arising from the lack of size consistency in QSCI, the intermolecular interaction energy has instead been calculated using the following equation,

$$E_{\rm int} = E_{\rm AB} - E_{\rm A \cdots B} \tag{2}$$

Here, $E_{A...B}$ denotes the energy of the dimer composed of monomers A and B at a sufficiently large inter-monomer distance. Hereafter, we refer to the approach based on equation (2) as the "dimer approach". In 2025, Kaliakin and coworkers reported QSCI-based calculations of intermolecular interaction energies for water and methane dimers using the dimer approach [19]. However, it is evident that the computational cost is lower for the supramolecular approach than for the dimer approach, since the size of the subspace Hamiltonian to be diagonalized is smaller for monomers than for the dimer. It is also important to note that if Slater determinants are sampled independently for different geometries, the electronic configurations included in the subspace Hamiltonian may differ between geometries, potentially resulting in discontinuities in the potential energy curve. In this work, we propose a size-consistent implementation of HSB-QSCI (sc-HSB-QSCI) to overcome these challenges.

II. THEORY

In conventional HSB-QSCI [10], Slater determinants used for subspace Hamiltonian diagonalization are sampled from quantum states generated by real-time evolution of an approximate wave function. To expand the subspace, measurement outcomes obtained at different

evolution times, $k\Delta t$ for $k \leq K$, are combined. For example, HSB-QSCI with K=3 indicates that the subspace Hamiltonian is constructed using the measurement results from quantum circuit executions at k=1, 2, and 3

A schematic illustration of subspace construction in sc-HSB-QSCI is shown in Figure 1. Note that the following subspace construction approach is not limited to HSB-QSCI and can be universally applied to any selected CI framework. The strategy of sc-HSB-QSCI is as follows: (1) Sample Slater determinants for the dimer in the localized molecular orbital basis. (2) For each sampled bit string, check the electronic configuration of the dimer. If the configuration involves only intra-monomer excitations, split the bit string into those corresponding to each monomer and add them to the respective monomer subspace in the localized molecular orbital basis. If intermonomer charge-transfer excitations are present, add the bit string to the dimer subspace without splitting. (3) Perform subspace Hamiltonian diagonalization for the monomers using the Slater determinants generated in the previous step. (4) The dimer subspace Hamiltonian is constructed by including all possible combinations of the electronic configurations from monomer 1 and monomer 2 subspaces, as well as the Slater determinants corresponding to charge-transfer excitations. With this approach, electronic configurations required for size consistency but not sampled are systematically added, thereby ensuring that size consistency is automatically satisfied.

III. COMPUTATIONAL CONDITIONS

As a proof-of-principle demonstration of sc-HSB-QSCI, we performed numerical simulations on a classical computer. The target systems included a dimer of square tetrahydrogen (4H) clusters and hydrogen-bonded systems (FH dimer and FH-H₂O). The H-H bond length in the 4H cluster was set to 1.0583 Å (= 2.0 Bohr), and the 8H cluster was constructed by placing two 4H clusters in a cuboid arrangement with an inter-monomer distance of 100 Å. Note that this system has previously been used to investigate size consistency in VQE with a unitary coupled cluster singles and doubles (UCCSD) ansatz [33], and in QPE [34]. The localized molecular orbitals of the 8H cluster were manually generated by taking appropriate linear combinations of RHF/STO-3G [35] canonical orbitals. For sc-HSB-QSCI, all molecular orbitals were included in the Hamiltonian simulation, and the interaction energies were compared with those from fullconfiguration interaction (full-CI) calculations.

For the hydrogen-bonded systems, geometry optimizations of the dimers were performed at the PBE0 [36]/aug-cc-pVDZ [37, 38] level of theory. No imaginary vibrational frequencies were obtained at the optimized structure. The optimized geometries are shown in Figure 2, and the corresponding Cartesian coordinates are provided in Tables S1 and S2 in the Supporting Informa-

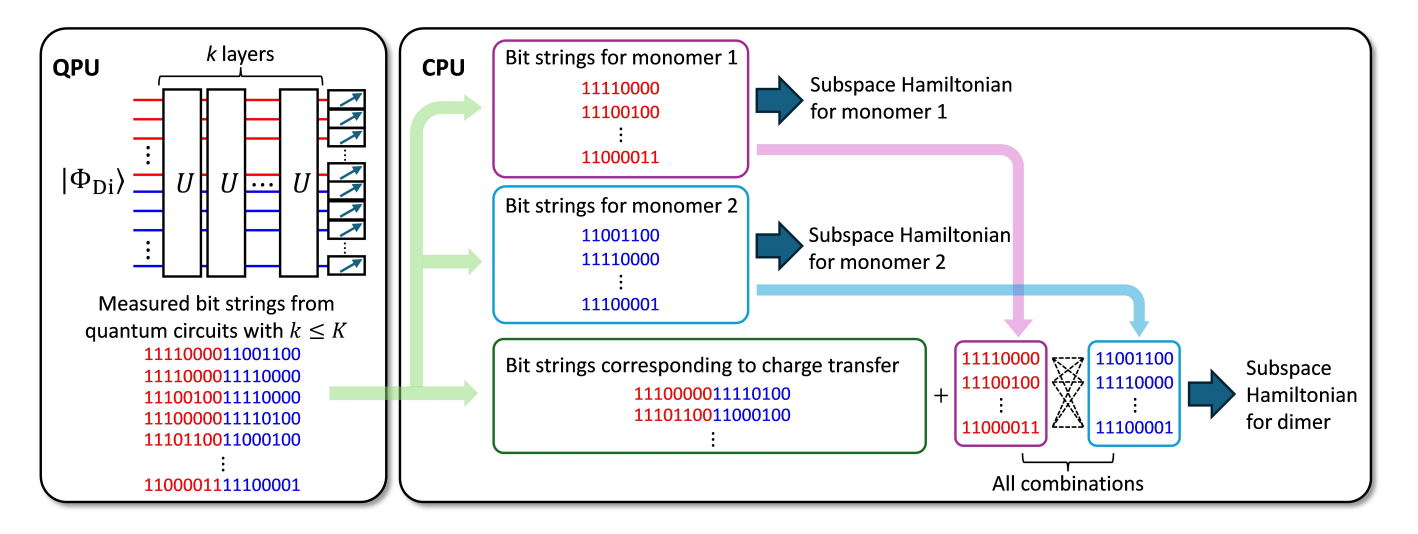


FIG. 1. Schematic illustration of subspace generation in sc-HSB-QSCI. $|\Phi_{\text{Di}}\rangle$ represents an approximate wave function for the dimer, and U is a time evolution operator $U = e^{-iHt}$.

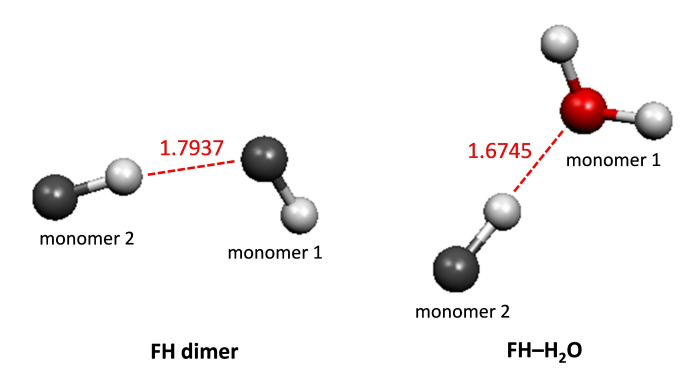


FIG. 2. PBE0/aug-cc-pVDZ optimized geometry of the FH dimer and FH-H₂O. Red dotted lines represent hydrogen bonds, and values in red denote intermolecular distances in units of $\mathring{\rm A}$.

tion. For monomer calculations, we used the optimized geometry for the dimer without further performing geometry optimization of the monomers. To assess size consistency, we also generated geometries for the dimers without inter-monomer interaction by increasing the intermonomer distance to 100 Å. Localized molecular orbitals for both dimers and monomers were generated using the Pipek-Mezey method [39] at the RHF/aug-cc-pVDZ level. In the sc-HSB-QSCI simulations, only valence orbitals were considered, with active space sizes of (16e. 100) for the FH dimer, (8e, 50) for the FH monomer, (16e, 11o) for the FH-H₂O, and (8e, 6o) for the H₂O. Here, (Ne, Mo) indicates an active space consisting of N electrons and M molecular orbitals. The active orbitals for the monomers and dimers of the FH dimer and FH-H₂O are shown in Figure S2 in Supporting Information. All DFT and RHF calculations were performed using the GAMESS-US program package [40].

Numerical simulations for sc-HSB-QSCI were per-

formed using our in-house Python3 code, developed with the OpenFermion [41], Cirq [42], and PyCI [43] libraries. Details of the HSB-QSCI implementation can be found in Reference [10]. The Jordan-Wigner transformation [44] was used for fermion-qubit encoding. The RHF wave function served as the initial state for time evolution, and the quantum circuit for the time evolution operator $U = e^{-iH\Delta t}$ with $\Delta t = 1$ was constructed using the second-order Trotter-Suzuki decomposition with a single Trotter step. Unless otherwise noted, the number of shots for quantum circuit execution was set to 1×10^4 , and K is varied from 1 to 5 and 10. In sc-HSB-QSCI, symmetry completion [10] was performed prior to constructing the subspace Hamiltonian matrix. In this step, any openshell Slater determinants required to span the eigenfunctions of the electron spin S^2 operator were added if miss-

For the hydrogen-bonded FH dimer and ${\rm FH-H_2O}$ systems, we also calculated intermolecular interaction energies using HCI in conjunction with the propose approach. The HCI calculations were performed using the PyCI [43] library.

IV. RESULTS AND DISCUSSION

A. Size consistency of sc-HSB-QSCI

Here, we numerically demonstrate that the sc-HSB-QSCI method satisfies the size consistency condition, using the 4H cluster as the monomer. The square 4H cluster is a well-known strongly correlated system [45], with a ground-state wave function exhibiting significant multi-configurational character. Using the STO-3G basis set [35], the full-CI dimensions are 12 and 178 for the monomer (4H cluster in the D_{2h} point group) and the dimer (8H cluster in the C_{2v} point group), respectively.

TABLE I. Sc-HSB-QSCI, RHF, and full-CI energies for the 8H (dimer) and 4H (monomer) clusters, in units of Hartree. The numbers in parenthesis indicate the number of Slater determinants included in the subspace Hamiltonian diagonalization.

\overline{K}	E(dimer)	E(monomer 1)	E(monomer 2)
1	-3.652202 (98)	-1.816720 (8)	-1.835483(8)
2	-3.862635 (124)	-1.933870(9)	-1.928764(10)
3	-3.862635 (124)	-1.933870(9)	-1.928764(10)
4	-3.862664 (134)	-1.933900(10)	-1.928764(10)
5	-3.862664 (134)	-1.933900 (10)	-1.928764(10)
RHF	-3.553541(1)	-1.776770(1)	-1.776770(1)
full-CI	-3.878863 (178)	-1.939432(12)	-1.939432(12)

TABLE II. Intermolecular interaction energies for the FH dimer and FH–H₂O at an inter-monomer distance of 100 Å, calculated using sc-HSB-QSCI and org-HSB-QSCI, in units of kcal mol⁻¹.

Molecule	K	sc-HSB-QSCI	org-HSB-QSCI
FH dimer	1	0.000	0.016
	2	0.000	0.016
	3	0.000	0.016
	4	0.000	0.013
	5	0.000	0.007
$FH-H_2O$	1	0.000	0.095
	2	0.000	0.046
	3	0.000	0.040
	4	0.000	0.040
	5	0.000	0.031

Owing to the small system size, sc-HSB-QSCI calculations were performed with 10 shots for each k. The results are summarized in Table I. The computed $E_{\rm int}$ values are less than 1×10^{-7} Hartree for all K. The small deviations of $E_{\rm int}$ from zero arize from rounding errors in the one- and two-electron integrals. These results clearly demonstrate the size consistent nature of sc-HSB-QSCI.

Next, we numerically investigated size consistency in the FH dimer and FH-H₂O systems using both sc-HSB-QSCI and the original form of HSB-QSCI (org-HSB-QSCI). As discussed above, org-HSB-QSCI is not size consistent, and the interaction energy can be nonzero even when the intermolecular distance is sufficiently large. In this study, we used geometries with an intermolecular distance of 100 Å. The calculated interaction energies are summarized in Table II, and total energies and the number of Slater determinants in the subspace are provided in Tables S3 and S4 in the Supporting Information. Sc-HSB-QSCI yielded an interaction energy E_{int} = $0.000 \text{ kcal mol}^{-1}$ for all K, whereas org-HSB-QSCI gave nonzero interaction energies. The error in $E_{\rm int}$ is slightly larger for FH-H₂O than for the FH dimer, suggesting that the violation of size consistency can increase as the number of active orbitals grows. In all systems under study, the number of sampled charge-transfer excited Slater determinants was zero.

B. Intermolecular interaction energies of hydrogen-bonded FH dimer and FH-H₂O

Lastly, we examine the intermolecular interaction energy calculations of the hydrogen-bonded FH dimer and FH-H₂O. Hydrogen bonding is one of the most important intermolecular interactions, particularly in biomolecules. Here, we compare interaction energies calculated using the supramolecular approach with sc-HSB-QSCI and org-HSB-QSCI, as well as the dimer approach with org-HSB-QSCI. The numerical simulation results, together with RHF and CAS-CI interaction energies, are summarized in Table III, and the total energies are listed in Tables S5 and S6 in the Supporting Information. Sc-HSB-QSCI yields larger interaction energies in absolute value and smaller errors relative to the CAS-CI values compared to org-HSB-QSCI. Org-HSB-QSCI using the dimer approach gave interaction energies comparable to those obtained with sc-HSB-QSCI, although its computational cost is higher than that of the supramolecular approach. At K = 10, sc-HSB-QSCI gave interaction energies with deviations of 0.012 and 0.038 kcal mol^{-1} from the CAS-CI values for the FH dimer and FH-H₂O, respectively. The number of Slater determinants included in the subspace Hamiltonian diagonalization for the dimer is 458 and 4150 for the FH dimer and FH-H₂O, respectively, which should be compared to 2025 and 27225, respectively, at the CAS-CI level of theory.

Table S7 in the Supporting Information presents the classification of bit strings sampled by the quantum computer into those corresponding to intra-monomer excited determinants and those representing inter-monomer charge-transfer excited determinants. Whether intra-monomer excitation or inter-monomer charge-transfer excitation is sampled more frequently depends on the duration of the time evolution. As k increases, the probability of sampling charge-transfer excitation becomes higher. This indicates that longer time evolution is important for accurately obtaining intermolecular interaction energies using sc-HSB-QSCI.

Since our size-consistent implementation is applicable to other selected CI frameworks, we applied our proposed scheme to heat-bath CI (HCI) [46]. Details of the numerical simulations are provided in subsection C of the Supporting Information. The size consistent HCI (sc-HCI) yielded intermolecular interaction energies slightly closer to the CAS-CI values than those obtained with sc-HSB-QSCI, indicating that sc-HCI achieves a more compact wave function expansion for a given level of accuracy. As discussed in our previous work [10], HSB-QSCI may sample Slater determinants that are important for excited states rather than the ground state. Therefore, screening out unimportant Slater determinants from the subspace is essential for obtaining a more compact wave function expansion in sc-HSB-QSCI, which remains one of the most significant challenges in QSCI. Nevertheless, the approach proposed in this study significantly improves the applicability of selected CI methods to intermolecu-

TABLE III. Intermolecular interaction energies of the hydrogen-bonded FH dimer and FH–H₂O, calculated using the supramolecular approach with sc-HSB-QSCI and org-HSB-QSCI, as well as the dimer approach with org-HSB-QSCI, in units of kcal mol⁻¹.

C4	V	Supramolec	ular approach	Dimer approach	RHF	CACOL
System	K	$sc ext{-HSB-QSCI}$	org-HSB-QSCI	org-HSB-QSCI	ппг	CAS-CI
FH dimer	1	-4.030	-4.002	-4.019		
	2	-4.037	-4.011	-4.027		
	3	-4.043	-4.020	-4.036	-3.971	-4.071
	4	-4.055	-4.040	-4.054	-5.971	-4.071
	5	-4.056	-4.041	-4.048		
	10	-4.059	-4.049	-4.053		
$FH-H_2O$	1	-8.450	-8.140	-8.234		
	2	-8.497	-8.402	-8.447		
	3	-8.687	-8.600	-8.640	-7.902	-8.786
	4	-8.695	-8.617	-8.658	-7.902	-0.700
	5	-8.717	-8.674	-8.705		
	10	-8.748	-8.717	-8.741		

lar interaction energy calculations.

V. CONCLUSION

In summary, we have developed a size-consistent implementation of Hamiltonian simulation-based quantum-selected configuration interaction (sc-HSB-QSCI) for intermolecular interaction energy calculations based on the supramolecular approach. The size consistency of the proposed method was confirmed through numerical simulations of the 8H cluster, FH dimer, and FH-H₂O systems with an inter-monomer distance of 100 Å, all yielding zero interaction energies. Interaction energies of intermolecular hydrogen bonds in the FH dimer and FH-H₂O were also calculated with sc-HSB-QSCI, and the results agreed with the CAS-CI interaction energies in the same active space with errors of only 0.012 and 0.038 kcal mol⁻¹ for the FH dimer and FH-H₂O, respectively. During the sampling procedure, intra-monomer excited con-

figurations are predominantly sampled in the early stage of real-time evolution, while the probability of sampling charge-transfer excited configurations increases at later stages. This trend indicates that extended real-time evolution is essential for accurately computing intermolecular interaction energies with sc-HSB-QSCI.

Apart from the supramolecular approach, size consistency is also crucial in other contexts, such as the fragment molecular orbital method [47, 48] and the ONIOM (our own N-layer integrated molecular orbitals and molecular mechanics) method [49, 50]. Applying the sc-HSB-QSCI method to these problems remains an important avenue for future research.

VI. ACKNOWLEDGMENTS

K.S. thanks Dr. Yuhei Tachi and Dr. Hiroyuki Tezuka for useful discussions.

D. S. Abrams and S. Lloyd. Quantum algorithm providing exponential speed increase for finding eigenvalues and eigenvectors. *Phys. Rev. Lett.*, 83:5162–5165, 1999.

^[2] A. Aspuru-Guzik, A. D. Dutoi, P. J. Love, and M. Head-Gordon. Simulated quantum computation of molecular energies. *Science*, 309:1704–1707, 2005.

^[3] M. A. Nielsen and I. L. Chuang. Quantum Computation and Quantum Information: 10th Anniversary Edition. Cambridge University Press, 2010.

^[4] A. Peruzzo, J. McClean, P. Shadbolt, M.-H. Yung, X.-Q. Zhou, P. J. Love, A. Aspuru-Guzik, and J. L. O'Brien. A variational eigenvalue solver on a photonic quantum processor. *Nat. Comm.*, 5:4213, 2014.

^[5] J. F. Gonthier, M. D. Radin, C. Buda, E. J. Doskocil, C. M. Abuan, and J. Romero. Measurements as a roadblock to near-term practical quantum advantage in chemistry: Resource analysis. *Phys. Rev. Res.*, 4:033154, 2022.

^[6] J. R. McClean, S. Boixo, V. N. Smelyanskiy, R. Babbush, and H. Neven. Barren plateaus in quantum neural network training landscapes. *Nat. Comm.*, 9:4812, 2018.

^[7] K. Kanno, M. Kohda, R. Imai, S. Koh, K. Mitarai, W. Mizukami, and Y. O. Nakagawa. Quantum-selected configuration interaction: classical diagonalization of Hamiltonians in subspaces selected by quantum computers. arXiv:2302.11320.

^[8] M. Motta, K. J. Sung, K. B. Whaley, M. Head-Gordon, and J. Shee. Bridging physical intuition and hardware efficiency for correlated electronic states: the local unitary cluster Jastrow ansatz for electronic structure. *Chem.* Sci., 14:11213–11227, 2023.

^[9] J. Robledo-Moreno, M. Motta, H. Haas, A. Javadi-Abhari, P. Jurcevic, W. Kirby, S. Martiel, K. Sharma, S. Sharma, T. Shirakawa, I. Sitdikov, R.-Y. Sun, K. J. Sung, M. Takita, M. C. Tran, S. Yunoki, and A. Mez-

- zacapo. Chemistry beyond the scale of exact diagonalization on a quantum-centric supercomputer. *Sci. Adv.*, 11:eqdu9991, 2025.
- [10] K. Sugisaki, S. Kanno, T. Itoko, R. Sakuma, and N. Yamamoto. Hamiltonian simulation-based quantumselected configuration interaction for large-scale electronic structure calculations with a quantum computer. *Phys. Chem. Chem. Phys.*, 27:20869–20884, 2025.
- [11] S. Kanno, K. Sugisaki, H. Nakamura, H. Yamauchi, R. Sakuma, T. Kobayashi, Q. Gao, and N. Yamamoto. Tensor-based quantum phase difference estimation for large-scale demonstrations. *Proc. Natl. Acad. Soc.* U.S.A., 122:e2425026122, 2025.
- [12] M. Mikkelsen and Y. O. Nakagawa. Quantum-selected configuration interaction with time-evolved state. *Phys. Rev. Res.*, 7:043043, 2025.
- [13] J. Yu, J. Robledo Moreno, J. T. Iosue, L. Bertels, D. Claudino, B. Fuller, P. Groszkowski, T. S. Humble, P. Jurcevic, W. Kirby, T. A. Maier, M. Motta, B. Pokharel, A. Seif, A. Shehata, K. J. Sung, M. C. Tran, V. Tripathi, A. Mezzacapo, and K. Sharma. Quantumcentric algorithm for sample-based Krylov diagonalization. arXiv:2501.09702.
- [14] S. Piccinelli, A. Baiardi, M. Rossmannek, A. C. Vazquez, F. Tacchino, S. Mensa, E. Altamura, A. Alavi, M. Motta, J. Robledo-Moreno, W. Kirby, K. Sharma, A. Mezzacapo, and I. Tavernelli. Quantum chemistry with provable convergence via randomized sample-based quantum diagonalization. arXiv:2508.02578.
- [15] T. Weaving, A. Mingare, A. Ralli, and P. V. Coveney. Towards compact wavefunctions from quantum-selected configuration interaction.
- [16] Y. O. Nakagawa, M. Kamoshita, W. Mizukami, S. Sudo, and Y. Ohnishi. ADAPT-QSCI: adaptive construction of an input state for quantum-selected configuration interaction. J. Chem. Theory Comput., 20:10817–10825, 2024.
- [17] I. Liepuoniute, K. D. Doney, J. Robledo Moreno, J. A. Job, W. S. Friend, and G. O. Jones. Quantum-centric computational study of methylene singlet and triplet states. J. Chem. Theory Comput., 21:5062–5070, 2025.
- [18] L. Nützel, A. Gresch, L. Hehn, L. Marti, R. Freund, A. Steiner, C. D. Marciniak, T. Eckstein, N. Stockinger, S. Wolf, T. Monz, M. Kühn, and M. J. Hartmann. Solving an industrially relevant quantum chemistry problem on quantum hardware. *Quantum Sci. Technol.*, 10:015066, 2025.
- [19] D. Kaliakin, A. Shajan, F. Liang, J. Robledo Moreno, Z. Li, A. Mitra, M. Motta, C. Johnson, A. A. Saki, S. Das, I. Sitdikov, A. Mezzacapo, and K. M. Merz Jr. Accurate quantum-centric simulations of intermolecular interactions. *Comm. Phys.*, 8:396, 2025.
- [20] S. Barison, J. Robledo Moreno, and M. Motta. Quantumcentric computation of molecular excited states with extended sample-based quantum diagonalization. *Quantum Sci. Technol.*, 10:025034, 2025.
- [21] A. Shajan, D. Kaliakin, A. Mitra, J. Robledo Moreno, Z. Li, M. Motta, C. Johnson, A. A. Saki, S. Das, I. Sitdikov, A. Mezzacapo, and K. M. Merz. Toward quantumcentric simulations of extended molecules: sample-based quantum diagonalization enhanced with density matrix embedding theory. J. Chem. Theory Comput., 21:6801– 6810, 2025.

- [22] P. Reinholdt, K. M. Ziems, E. R. Kjellgren, S. Coriani, S. P. A. Sauer, and J. Kongsted. Critical limitations in quantum-selected configuration interaction methods. J. Chem. Theory Comput., 21:6811–6822, 2025.
- [23] D. Kaliakin, A. Shajan, F. Liang, and K. M. Merz Jr. Implicit solvent sample-based quantum diagonalization. J. Phys. Chem. B, 129:5788–5796, 2025.
- [24] N. Bauer, K. Yeter-Aydeniz, and G. Siopsis. Efficient quantum chemistry calculations on noisy quantum hardware. arXiv:2503.02778.
- [25] A. Duriez, P. C. Carvalho, M. A. Barroca, F. Zipoli, B. Jaderberg, R. N. B. Ferreira, K. Sharma, A. Mezzacapo, B. Wunsch, and M. Steiner. Computing band gaps of periodic materials via sample-based quantum diagonalization. arXiv:2503.10901.
- [26] T. Ohgoe, H. Iwakiri, K. Ichikawa, S. Koh, and M. Kohda. Quantum computation of a quasiparticle band structure with the quantum-selected configuration interaction. J. Phys. Soc. Jpn., 94:114002, 2025.
- [27] K. Nogaki, S. Backes, T. Shirakawa, S. Yunoki, and R. Arita. Symmetry-adapted sample-based quantum diagonalization: application to lattice model. arXiv:2505.00914.
- [28] T. M. Bickley, A. Mingare, T. Weaving, M. W. de la Bastida, S. Wan, M. Nibbi, P. Seitz, A. Ralli, P. J. Love, M. Chung, M. H. Vera, L. Schulz, and P. V. Coveney. Extending quantum computing through subspace, embedding and classical molecular dynamics techniques. arXiv:2505.16796.
- [29] Y. Chen, R. Wu, M. H. Cheng, and M.-H. Hsieh. Neural network assisted fermionic compression encoding: a lossy-QSCI framework for resource-efficient ground-state simulations. *Phys. Rev. Res.*, 2025.
- [30] S. Shivpuje, T. P. Gujarati, R. Van, F. C. Pickard IV, T. Friedhoff, I. Liepuoniute, W. Davis, G. O. Jones, and A. Galda. Sample-based quantum diagonalization methods for modeling the photochemistry and diazirine and diazo compounds. arXiv:2510.00484.
- [31] T. Smith, T. P. Gujarati, M. Motta, B. Link, I. Liepuoniute, T. Friedhoff, H. Nishimura, N. Nguyen, K. S. Williams, J. Robledo Moreno, C. Johnson, K. J. Sung, A. A. Saki, and M. Kagele. Quantum-centric simulation of hydrogen abstraction by sample-based quantum diagonalization and entanglement forging, arXiv:2508.08229.
- [32] H. Matsuyama and Y. Yamashiro. Sampling-based quantum optimization algorithm with quantum relaxation. arXiv:2504.12629.
- [33] K. Sugisaki, T. Nakano, and Y. Mochizuki. Size-consistency and orbital-invariance issues revealed by VQE-UCCSD calculations with the FMO scheme. J. Comp. Chem., 45:2204–2213, 2024.
- [34] K. Sugisaki. Does the full configuration interaction method based on quantum phase estimation with Trotter decomposition satisfy the size consistency condition? AIP Adv., 14:095021, 2024.
- [35] W. J. Hehre, R. F. Stewart, and J. A. Pople. Self-consistent molecular-orbital methods. I. use of Gaussian expansion of Slater-type atomic orbitals. *J. Chem. Phys.*, 51:2657–2664, 1969.
- [36] C. Adamo and V. Barone. Toward reliable density functional methods without adjustable parameters: the PBE0 model. J. Chem. Phys., 110:6158-6170, 1999.
- [37] T. H. Dunning Jr. Gaussian basis sets for use in correlated molecular calculations. I. the atoms boron through

- neon and hydrogen. J. Chem. Phys., 90:1007-1023, 1989.
- [38] R. A. Kendall, T. H. Dunning Jr., and R. J. Harrison. Electron affinities of the first-row atoms revisited. systematic basis sets and wave functions. J. Chem. Phys., 96:6796–6806, 1992.
- [39] J. Pipek and P. G. Mezey. A fast intrinsic localization procedure applicable for ab initio and semiempirical linear combination of atomic orbital wave functions. *J. Chem. Phys.*, 90:4916–4926, 1989.
- [40] G. M. J. Barca, C. Bertoni, L. Carrington, D. Datta, N. De Silva, J. Emiliano Deustua, D. G. Fedorov, J. R. Gour, A. O. Gunina, E. Guidez, T. Harville, S. Irle, J. Ivanic, K. Kowalski, S. S. Leang, H. Li, W. Li, J. J. Lutz, I. Magoulas, J. Mato, V. Mironov, H. Nakata, B. Q. Pham, P. Piecuch, D. Poole, S. R. Pruitt, A. P. Rendell, L. B. Roskop, K. Ruedenberg, T. Sattasathuchana, M. W. Schmidt, J. Shen, L. Slipchenko, M. Sosonkina, V. Sundriyal, A. Tiwari, J. L. Galvez Vallejo, B. Westheimer, M. Wloch, P. Xu, F. Zahariev, and M. S. Gordon. Recent developments in the general atomic and molecular electronic structure system. J. Chem. Phys., 152:154102, 2020.
- [41] J. R. McClean, N. C. Rubin, K. J. Sung, I. D. Kivlichan, X. Bonet-Monroig, Y. Cao, C. Dai, E. Schuyler Fried, C. Gidney, B. Gimby, P. Gokhale, T. Häner, T. Hardikar, V. Havliček, O. Higgott, C. Huang, J. Izaac, Z. Jiang, X. Liu, S. McArdle, M. Neeley, T. O'Brien, B. O'Gorman, I. Ozfidan, M. D. Radin, J. Romero, N. P. D. Sawaya, B. Senjean, K. Setia, S. Sim, D. S. Steiger, M. Steudtner, Q. Sun, W. Sun, D. Wang, F. Zhang, and R. Babbush. OpenFermion: the electronic structure package for quantum computers. Quantum Sci. Technol., 5:034014, 2020.
- [42] Cirq Developers. Cirq (v1.6.0). Zenodo, 2022.
- [43] M. Richer, G. Sánchez-Díaz, M. Martínez-González, V. Chuiko, T. D. Kim, A. Tehrani, S. Wang, P. B. Gaikwad, C. E. V. de Moura, C. Masschelein, R. A. Miranda-Quintana, A. Gerolin, F. Heider-Zadeh, and P. W. Ayers. PyCI: a Python-scriptable library for arbitrary determinant CI. J. Chem. Phys., 161:132502, 2024.
- [44] P. Jordan and E. Wigner. Über das paulische äquivalenzverbot. Z. Phys., pages 631–651, 1928.
- [45] J. Paldus, P. Piecuch, L. Pylypow, and B. Jeziorski. Application of Hilbert-space coupled-cluster theory to simple (H₂)₂ model systems: planar models. *Phys. Rev. A*, 47:2738–2782, 1993.
- [46] A. A. Holmes, N. M. Tubman, and C. J. Umrigar. Heat-bath configuration interaction: an efficient selected configuration interaction algorithm inspired by heat-bath sampling. J. Chem. Theory Comput., 12:3674–3680, 2016.
- [47] K. Kitaura, E. Ikeo, T. Asada, T. Nakano, and M. Ue-bayashi. Fragment molecular orbital method: an approximate computational method for large molecules. *Chem. Phys. Lett.*, 313:701–706, 1999.
- [48] Y. Mochizuki, S. Tanaka, and K. Fukuzawa, editors. Recent Advances of the Fragment Molecular Orbital Method: Enhanced Performance and Applicability. Springer, 2022.
- [49] M. Svensson, S. Humbel, R. D. J. Froese, T. Matsubara, S. Sieber, and K. Morokuma. ONIOM: a multilayered integrated MO + MM method for geometry optimizations and single point energy predictions. a test for Diels-Alder reactions and Pt(P(t-Bu)₃)₂) + H₂ oxidative addition. J. Phys. Chem., 100:19357-19363, 1996.

[50] L. W. Chung, W. M. C. Sameera, R. Ramozzi, A. J. Page, M. Hatanaka, G. P. Petrova, T. V. Harris, X. Li, Z. Ke, F. Liu, H.-B. Li, L. Ding, and K. Morokuma. The ONIOM method and its applications. *Chem. Rev.*, 115:5678–5796, 2015.

VII. SUPPORTING INFORMATION

A. Cartesian coordinates

TABLE S1. Cartesian coordinates of the PBE0/aug-cc-pVDZ optimized geometry for the hydrogen-bonded FH dimer, given in units of Å.

Atom	X	Y	Z
F	-0.355909	0.404037	0.199053
Η	0.112061	-0.309544	-0.156637
\mathbf{F}	-3.008949	-0.078707	-0.096402
Η	-2.130203	0.184214	0.053986

TABLE S2. Cartesian coordinates of the PBE0/aug-cc-pVDZ optimized geometry for the hydrogen-bonded FH-H₂O, given in units of Å.

Atom	X	Y	Z
O	-2.451734	0.852831	-0.885154
Н	-1.585104	0.709253	-0.491503
\mathbf{H}	-2.774601	1.674026	-0.500774
\mathbf{F}	-4.071275	-1.154030	-0.438062
Н	-3.491540	-0.434027	-0.626687

B. Relationship between the number of quantum circuit repetitions and size consistency

Here, we demonstrate that the number of quantum circuit repetitions must increase exponentially with system size in order to approximately satisfy the size consistency condition in QSCI. For clarity, our discussion focuses on the original QSCI and assumes access to a state preparation oracle capable of generating the CAS-CI wave function.

$$Prep|0\rangle^{\otimes n} = |\Psi\rangle = \sum_{j} c_{j} |\psi_{j}\rangle$$

Here, $|\Psi\rangle$ denotes the CAS-CI wave function of the target electronic state, and $\{|\psi_j\rangle\}$ represents the set of Slater determinants. In addition, we assume an ideal measurement scenario in which each Slater determinant $|\psi_j\rangle$ is sampled once for every $1/|c_j|^2$ measurements performed.

Let us consider a dimer composed of two monomers with no intermolecular interactions. In this case, the wave function of the dimer can be expressed as the direct product of the wave functions of the individual monomers, as shown below.

$$|\Psi_{\mathrm{dimer}}\rangle = \sum_{jk} c_j c_k |\psi_j\rangle \otimes |\psi_k\rangle$$

Based on this, sampling the Slater determinant represented as the direct product $|\psi_j\rangle\otimes|\psi_j\rangle$ requires executing

the quantum circuit $1/|c_j|^4$ times.

C. Size-consistent implementation for heat-bath CI

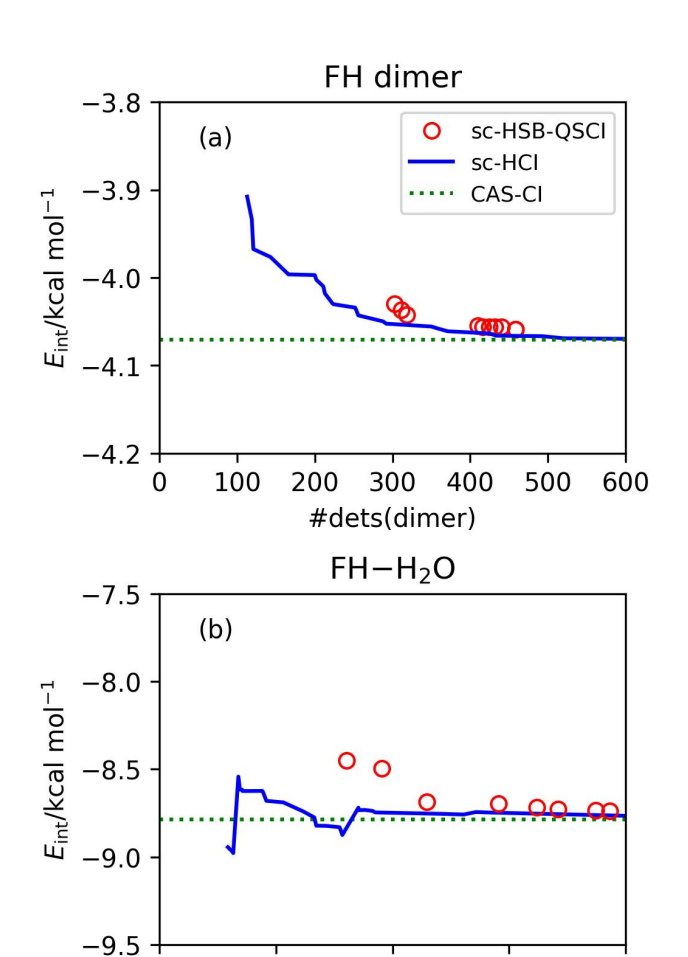


FIG. S1. Number of dimer Slater determinants included in the subspace Hamiltonian versus intermolecular interaction energy obtained from sc-HCI and sc-HSB-QSCI in (a) FH dimer and in (b) FH- $\rm H_2O$.

2000

#dets(dimer)

3000

4000

1000

0

As discussed in the Theory section, the size-consistent implementation proposed in this study is applicable to any selected CI framework. Here, we examine its application to heat-bath CI (sc-HCI). In sc-HCI, we first perform HCI calculations for the dimer, and the resulting Slater determinants are used to construct the subspaces for both the monomers and the dimer. In this work, HCI was carried out with threshold values ε ranging from 1.0×10^{-4} to 5.0×10^{-3} . Figure S1 plots the number of dimer Slater determinants against the intermolecular interaction energies calculated using both sc-HCI as well as sc-HSB-QSCI. Notably, sc-HCI yielded intermolecular interaction energies that are closer to the CAS-CI values than those obtained with sc-HSB-QSCI.

D. Localized molecular orbitals and sc-HSB-QSCI results

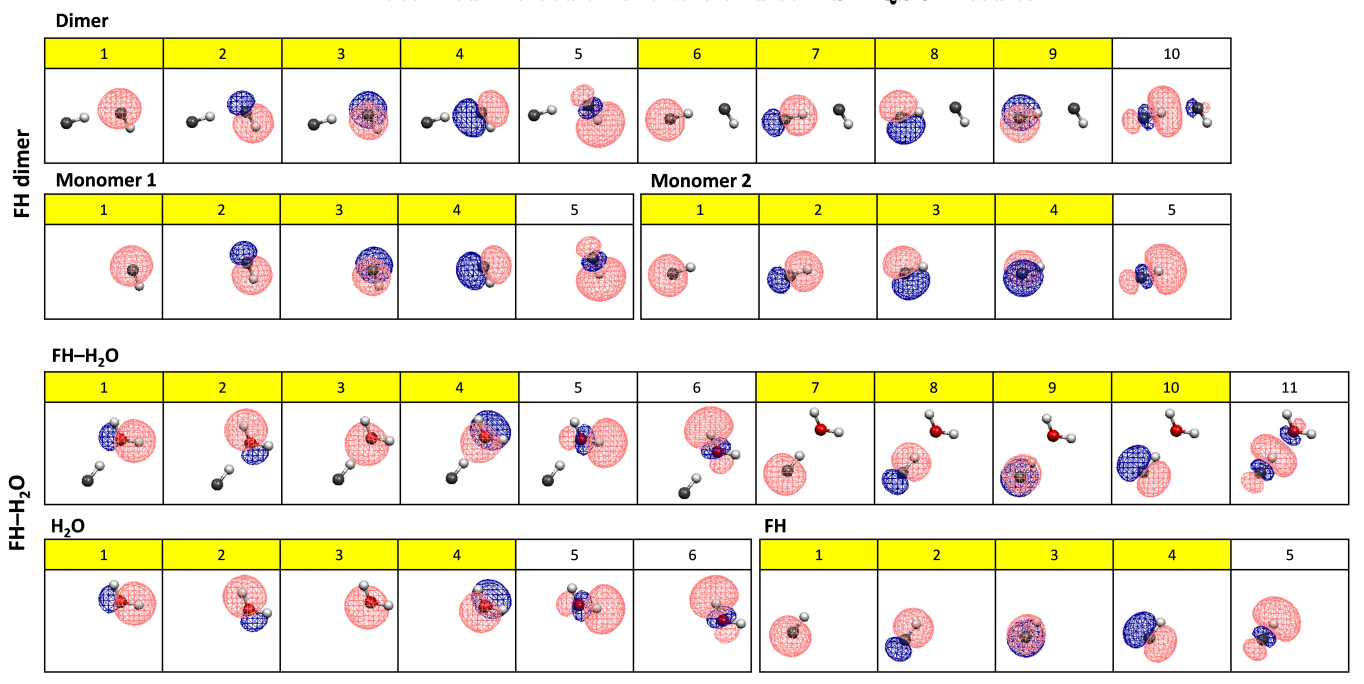


FIG. S2. Localized molecular orbitals of FH dimer and FH-H $_2$ O used as active space for HSB-QSCI. Orbitals with yellow highlights are occupied ones, and those without highlight are unoccupied.

TABLE S3. Sc-HSB-QSCI, org-HSB-QSCI, RHF, and full-CI energies of the FH dimer at an intermolecular distance of 100 Å, in units of Hartree. The numbers in parenthesis indicate the number of Slater determinants in the subspace.

K		sc-HSB-QSCI			org-HSB-QSCI	
Λ	E(dimer)	E(monomer 1)	E(monomer 2)	E(dimer)	E(monomer 1)	E(monomer 2)
1	-200.097212 (139)	-100.048655 (11)	-100.048558 (11)	-200.097187(39)	-100.048655 (11)	-100.048558(11)
2	-200.097212 (139)	-100.048655 (11)	-100.048558 (11)	-200.097187(48)	-100.048655 (11)	-100.048558(11)
3	-200.097212 (139)	-100.048655 (11)	-100.048558 (11)	-200.097187(48)	-100.048655 (11)	-100.048558(11)
4	-200.097212 (139)	-100.048655 (11)	-100.048558 (11)	-200.097191(52)	-100.048655 (11)	-100.048558(11)
5	-200.097212 (139)	-100.048655 (11)	-100.048558 (11)	-200.097202(62)	-100.048655 (11)	-100.048558(11)
RHF	-200.065881(1)	-100.033096(1)	-100.032785(1)	-200.065881(1)	-100.033096(1)	-100.032785(1)
full-CI	$-200.097212 \ (2025)$	-100.048655 (25)	-100.048558 (25)	$-200.097212 \ (2025)$	-100.048655 (25)	-100.048558 (25)

TABLE S4. Sc-HSB-QSCI, org-HSB-QSCI, RHF, and full-CI energies of the FH-H $_2$ O at an intermolecular distance of 100 Å, in units of Hartree. The numbers in parenthesis indicate the number of Slater determinants in the subspace.

\overline{K}		sc-HSB-QSCI			org-HSB-QSCI	
Λ	E(dimer)	E(monomer 1)	E(monomer 2)	E(dimer)	E(monomer 1)	E(monomer 2)
1	-176.128580 (1327)	-76.080556 (95)	-100.048023 (11)	-176.128507 (198)	-76.080634 (86)	-100.048023(11)
2	-176.128687 (1394)	-76.080663 (100)	-100.048023 (11)	-176.128616 (213)	-76.080665 (99)	-100.048023(11)
3	-176.128697 (1433)	-76.080674 (103)	-100.048023 (11)	-176.128626 (218)	-76.080667 (107)	-100.048023(11)
4	-176.128703 (1545)	-76.080680 (111)	-100.048023 (11)	-176.128641 (246)	-76.080683 (119)	-100.048023(11)
5	-176.128710 (1629)	-76.080686 (117)	-100.048023 (11)	-176.128661 (301)	-76.080687 (121)	-100.048023 (11)
RHF	-176.072736(1)	-76.041090(1)	-100.031644(1)	-176.072736(1)	-76.041090(1)	-100.031644(1)
full-CI	$-176.128718 \ (27225)$	-76.080692 (225)	-100.048024 (25)	-176.128718 (27225)	-76.080692 (225)	-100.048024 (25)

TABLE S5. Sc-HSB-QSCI, org-HSB-QSCI, RHF, and full-CI energies of the hydrogen-bonded FH dimer, in units of Hartree. The numbers in parenthesis indicate the number of Slater determinants in the subspace.

		sc-HSB-QSCI			
N	E(dimer)	E(monomer 1)	E(monomer 2)	E(dimer)	
1	-200.103634(303)	-100.048655 (15)	-100.048558 (13)	-200.103590 (134)	
2	-200.103645(311)	-100.048655 (15)	-100.048558 (13)	-200.103605(156)	
3	-200.103655 (318)	-100.048655 (15)	-100.048558 (13)	-200.103618 (178)	
4	-200.103674(410)	-100.048655 (17)	-100.048558 (15)	-200.103651 (204)	
5	-200.103676 (416)	-100.048655 (17)	-100.048558 (15)	-200.103653 (216)	
10	-200.103681 (458)	-100.048655 (17)	-100.048558 (15)	-200.103665 (280)	
RHF	-200.072209(1)	-100.033096(1)	-100.032785(1)	-200.072209(1)	
full-CI	-200.103699 (2025)	-100.048655 (25)	-100.048558 (25)	-200.103699 (2025)	

TABLE S6. Sc-HSB-QSCI, org-HSB-QSCI, RHF, and full-CI energies of the hydrogen-bonded FH- $\rm H_2O$, in units of Hartree. The numbers in parenthesis indicate the number of Slater determinants in the subspace.

K		sc-HSB-QSCI				
	E(dimer)	E(monomer 1)	E(monomer 2)	E(dimer)		
1	-176.141994 (1608)	-76.080505(97)	-100.048023 (11)	-176.141629 (514)		
2	-176.142184 (1911)	-76.080621 (112)	-100.048023(11)	-176.142078 (685)		
3	-176.142490 (2293)	-76.080624(132)	-100.048023 (11)	-176.142395 (861)		
4	-176.142513 (2907)	-76.080634 (140)	-100.048023 (13)	-176.142439 (985)		
5	-176.142601 (3239)	-76.080686 (151)	-100.048023 (13)	-176.142533 (1197)		
10	-176.142652 (4150)	-76.080688 (184)	-100.048023 (13)	-176.142607 (1789)		
RHF	-176.085325(1)	-76.041090(1)	-100.031644(1)	-176.085325(1)		
full-CI	$-176.142717 \ (27225)$	-76.080693 (225)	-100.048023 (25)	-176.142717 (27225)		

TABLE S7. Number of sampled bit strings corresponding to intra-monomer excited and inter-monomer charge-transfer excited Slater determinants.

Molecule	K	Intra-monomer	Charge transfer
FH dimer	1	40	37
	2	46	51
	3	54	60
	4	66	74
	5	68	77
	10	87	102
$FH-H_2O$	1	117	84
	2	151	113
	3	184	160
	4	210	199
	5	235	241
	10	328	409